A Kilometer-Scale Coupled Atmosphere–Wave Forecasting System for the European Arctic

ERIN E. THOMAS,[a] MALTE MÜLLER,[a,b] PATRIK BOHLINGER,[c] YURII BATRAK,[a] AND NICHOLAS SZAPIRO[a]

[a] *Norwegian Meteorological Institute, Oslo, Norway*
[b] *Department of Geosciences, University of Oslo, Oslo, Norway*
[c] *Norwegian Meteorological Institute, Bergen, Norway*

ABSTRACT: Accurately simulating the interactions between the components of a coupled Earth modeling system (atmosphere, sea ice, and wave) on a kilometer-scale resolution is a new challenge in operational numerical weather prediction. It is difficult due to the complexity of interactive mechanisms, the limited accuracy of model components, and scarcity of observations available for assessing relevant coupled processes. This study presents a newly developed convective-scale atmosphere–wave coupled forecasting system for the European Arctic. The HARMONIE-AROME configuration of the ALADIN-HIRLAM numerical weather prediction system is coupled to the spectral wave model WAVEWATCH III using the OASIS3 model coupling toolkit. We analyze the impact of representing the kilometer-scale atmosphere–wave interactions through coupled and uncoupled forecasts on a model domain with 2.5-km spatial resolution. To assess the coupled model's accuracy and uncertainties we compare 48-h model forecasts against satellite observational products such as Advanced Scatterometer 10-m wind speed, and altimeter-based significant wave height. The fully coupled atmosphere–wave model results closely match both satellite-based wind speed and significant wave height observations as well as surface pressure and wind speed measurements from selected coastal station observation sites. Furthermore, the coupled model contains smaller standard deviation of errors in both 10-m wind speed and significant wave height parameters when compared to the uncoupled model forecasts. Atmosphere and wave coupling reduces the short-term forecast error variability of 10-m wind speed and significant wave height with the greatest benefit occurring for high wind and wave conditions.

SIGNIFICANCE STATEMENT: Accurately simulating the Earth system (atmosphere, sea ice, and wave) on a kilometer-scale resolution is a new challenge in numerical weather prediction. It is difficult due to the complexity of interactions between the atmosphere, ocean surface, and sea ice. Other obstacles in the development of a coupled forecasting system include the limited accuracy of individual model components as well as the limited availability of observations that represent coupled processes. This study presents a newly developed high-resolution atmosphere–wave coupled forecasting system for the European Arctic. We show the impact of representing kilometer-scale atmosphere–wave interactions and assess the accuracy of the coupled forecast model by comparing model results against satellite-based observations of 10-m wind speed and significant wave height. Results show the fully coupled atmosphere–wave forecasting system closely matches satellite observations of 10-m wind speed and significant wave height as well as measurements of wind speed from coastal observation sites. The coupled atmosphere–wave system also reduces the variability of forecast errors for both 10-m wind speed and significant wave height for high wind speeds and large wave magnitudes.

KEYWORDS: Arctic; Numerical weather prediction/forecasting; Model evaluation/performance

1. Introduction

The annual mean temperature of the Arctic has risen at an observed rate greater than 0.6°C per decade since the 1980s (Hansen et al. 2010; Comiso and Hall 2014; Karl et al. 2015; Huang et al. 2017). Furthermore, these trends are expected to continue with temperatures over the Svalbard archipelago are projected to increase by 10°C by the end of the twenty-first century (Hanssen-Bauer et al. 2018) under a high emission scenario. Rising temperatures have reduced annual mean Arctic sea ice extent by at least 4% per decade (Cavalieri and Parkinson 2012; Meredith et al. 2019), thus increasing areas of open ocean. With growing regions of open water in the Arctic, interactions between the atmosphere and ocean surface such as momentum, heat and moisture fluxes, will have increasingly strong influences on the development of high latitude weather patterns (Ricchi et al. 2016). Understanding these coupled interactions will greatly influence our ability to produce accurate Arctic forecasts.

Additionally, there is a demand for accurate short-range forecast products in Arctic regions due to expected increases in Arctic ship traffic from tourism and other activities (Hall and Saarinen 2010; Smith and Stephenson 2013; Dawson et al. 2017; Stocker et al. 2020). Improved Arctic forecasts would benefit many users in industries such as shipping, tourism, transportation, fishing, recreational activities, as well as sensitive coastal communities. Polar forecasting capabilities could be improved by explicitly representing air–sea interactions in

short-range numerical weather prediction (NWP) systems (Jung et al. 2016). Capturing these air–sea interactions can improve the forecast representation of severe weather conditions in the Arctic such as polar lows, cold air outbreaks, sea spray icing events, and dangerous instances of strong wind and large waves.

There are few examples of operational coupled atmosphere–wave forecasting systems. One such operational coupled system is the high-resolution version of the Integrated Forecasting System (IFS-HRES) operated by the European Centre for Medium-Range Weather Forecasts (ECMWF; Janssen 2004; Breivik et al. 2015). However, due to the global domain it is run at a non-convection-resolving spatial resolution of approximately 10 km. In addition, several studies highlight the benefit of performing atmosphere–wave coupling (Makin and Kudryavtsev 1999; Kudryavtsev et al. 1999). Wahle et al. (2017) demonstrates that coupling an atmospheric model with a Wave Model (WAM) improves wave forecasts in the North Sea. Wu et al. (2019) investigate ocean–wave–atmosphere interactions in the North Sea and Baltic Sea in a high resolution coupled model comprised of Weather Research and Forecasting (WRF) Model, WAVEWATCH III (WW3), and the Nucleus of European Modeling of the Ocean (NEMO). They determine that coupling processes are particularly important in coastal regions. Wu (2021) tests the impact of coupling at 5-km horizontal resolution during a polar low event associated with high winds in the Barents Sea and shows wave and ocean coupling impacts the model development of polar low intensity and track. Other examples of atmosphere–wave coupling include studies by Süld et al. (2015) and Rasheed et al. (2017), which perform direct, or in-line, two-way coupling with HARMONIE-AROME and the wave model WAM. Other studies show the added value of wave coupling in numerical weather prediction is of high importance during extreme wind events, such as hurricanes, to accurately estimate storm intensity and wind speed (Liu et al. 2011; Chen et al. 2013).

In traditional atmospheric forecast models, wind stress τ is estimated based on a bulk formula as follows:

$$\tau = \rho C_D U_{10}^2, \tag{1}$$

where ρ is the air density, C_D is the drag coefficient for momentum under neutral stratification, and U_{10} is the 10-m wind speed. The drag coefficient is typically parameterized based on the sea surface roughness length z_0:

$$C_D = \kappa^2 \ln\left(\frac{z}{z_0}\right)^{-2}, \tag{2}$$

where κ is the von Kármán constant, and z is defined as 10 m above sea level. The surface roughness length z_0 is calculated through the Charnock relationship:

$$z_0 = \frac{\alpha u^{*2}}{g}, \tag{3}$$

where α is the parameterized Charnock coefficient, $u*$ is the friction velocity, and g is the acceleration of gravity.

These bulk formulas estimate the surface roughness length in weather prediction models; however, they do not capture the influence of waves on surface roughness and thus could negatively impact the estimated surface wind speed and surface fluxes over open water in short-term forecasts. These wind–wave interactions can be critically important particularly in high wind or storm conditions (Liu et al. 2011; Chen et al. 2013; Zheng et al. 2016; Wu et al. 2019; Wu 2021). Additionally, it is important to capture these interactions in high latitude regions where surface fluxes can be large in magnitude and high wind events, such as polar lows, frequently occur (Isachsen et al. 2013; Stoll et al. 2020; Wu 2021). However, presently, no operational convection-permitting forecast models are coupled with wave models to capture these important surface interactions.

To our knowledge, there are currently no kilometer-scale, operational atmosphere–wave forecasting systems that are run in a fully coupled framework in order to capture rapidly changing and complex high latitude surface conditions. Here, we present a newly developed coupled NWP system containing a convective-scale atmospheric forecasting model coupled to a spectral wave model as the first step toward developing a fully coupled convective-permitting forecasting system for the European Arctic. The developments are building upon the Norwegian Meteorological Institute's operational convective-scale European Arctic weather prediction system (Müller et al. 2017a).

Coupling an atmospheric forecasting model with a wave model allows us to directly estimate the Charnock coefficient α based on the full wave spectrum, rather than use a constant or a parameterized bulk value. This can ultimately result in better representations of surface roughness, surface fluxes and low level wind speeds in short-term weather forecasts in our region of interest. To estimate the impact of wave coupling on the forecast system we compare coupled and uncoupled model forecasts against satellite products of ocean surface winds and significant wave height.

This paper is organized as follows: section 2 contains an overview of the atmosphere–wave coupled forecasting system and a description of the physical coupling process. Section 3 describes the experiential setup and methodology while section 4 presents the coupled NWP results, which include a comparison of the coupled system against satellite-based observations. Section 5 contains the conclusions and discussion.

2. Coupled forecast model description

a. HARMONIE-AROME

The atmospheric component of the coupled system described in this document is a regional, convective-scale weather forecasting system based on the HARMONIE-AROME NWP model Bengtsson et al. (2017). More specifically, the version used in the coupled framework presented here is built upon HARMONIE-AROME version cy43h2 beta7.

Embedded within HARMONIE-AROME is the surface model, SURFEX (Masson et al. 2013; Voldoire et al. 2017). SURFEX parameterizes surface processes and is responsible for all exchanges between surface and the lowest atmospheric

model level. Thus, the majority of the coupling processes implemented in the developed coupled forecasting system (see section 2c) take place within the SURFEX module.

The sea ice scheme used in our coupled model setup is the Simple Ice Scheme (SICE; Batrak et al. 2018). SICE is a one-dimensional thermodynamic sea ice parameterization scheme implemented as a subcomponent of SURFEX. Processes of ice formation are not represented in SICE; therefore, it requires an external ice concentration field to define ice-covered grid cells. In the current study, SICE is provided with the ice concentration from ECMWF IFS-HRES global operational forecasts.

We run HARMONIE-AROME on the AROME-Arctic domain, which has a horizontal resolution of 2.5 km, and uses a 1-min time step (Müller et al. 2017a). We test the coupled system with this configuration to match the configuration of the current operational forecasting system. The coupled system uses an upper air and surface data assimilation system as described in Müller et al. (2017b). In the present setup only conventional observations are used for data assimilation and remote sensing data from radars, GNSS, or satellites are not assimilated. To fully capture the two way coupling effects with the wave model, we use the ''COARE3.0'' sea surface flux parameterization scheme within SURFEX (Fairall et al. 2003; Le Moigne 2018).

b. WAVEWATCH III

The wave model used in the coupled forecasting system is the spectral wave model WAVEWATCH III, hereafter referred to as WW3, version 5.16 (WAVEWATCH III Development Group 2016).

For the coupled forecasting system, we define the WW3 domain to match the 2.5-km AROME-Arctic domain used by HARMONIE-AROME. WW3 is configured with a 5-min time step and a two-dimensional spectral resolution of 36 frequencies by 36 directions. The bathymetry used is the 2019 grid General Bathymetric Chart of the Oceans (GEBCO Bathymetric Compilation Group 2020), which is remapped onto the model grid. Two-dimensional wave spectra required for the lateral boundary conditions are taken from the ECMWF operational wave model forecasts.

WW3 provides a selection of different physics packages which allow the user to configure the model with the required level of complexity. In our coupled framework we used the ''ST3'' wind–wave input and dissipation physics package, which follows WAM4 physics and is based on Miles (1957), Janssen (1982), and Janssen (1991). We use the WAM4 equivalent physics package because it is computationally less expensive than higher-order schemes and is consistent with the physics used in the current operational wave model at the Norwegian Meteorological Institute. We allow for wave damping by sea ice where wave energy is dissipated by friction in the boundary layer below a continuous thin elastic plate of sea ice (Liu and Mollo-Christensen 1988; Liu et al. 1991; Ardhuin et al. 2015). A first evaluation of the wave attenuation by sea ice in the coupled system described here has been performed in Løken et al. (2020), which shows that WW3 represents the observed significant wave height and wave period within the marginal ice zone well. Additional wave model

settings in the coupled setup include bottom friction, wave reflection off sea ice and shorelines, and no sea ice scattering. A complete list of the exact WW3 model settings used in the coupled framework can be found in the appendix.

c. Coupling setup

There are two possible ways to couple two model components into a single forecasting system. The first method is via direct coupling. In this method the wave model is directly embedded into the atmospheric model and called as a subroutine, as was done by Süld et al. (2015) and Rasheed et al. (2017). The second method utilizes an external coupler to handle the exchange of information between two, independently running, model components. In the coupled forecasting system presented in this paper, we select the second method based on the following reasons:

1) The coupler can transform the exchanged fields between two model components as required, thus the models can use different temporal and spatial resolutions and domains, if necessary.
2) Direct control of the coupling frequency and the number of exchanged parameters is possible with the coupler.
3) Individual upgrades of the system's model components are possible as new versions become available in the future.

The external coupler used in our coupled forecast system is OASIS3-MCT (Valcke et al. 2015). OASIS3-MCT controls both temporal interpolation and spatial remapping of exchanged fields between HARMONIE-AROME and WW3. The physical coupling process represented in our coupled forecast model is described below.

WW3 calculates the Charnock parameter α based on the 2D wave spectrum as follows:

$$\alpha = \frac{\hat{\alpha}}{\sqrt{1 - \tau_w/\tau}}, \qquad (4)$$

where $\hat{\alpha}$ is the Charnock constant, τ_w is the wave supported stress, and τ is the total stress.

In the coupled setup we apply a similar momentum coupling strategy between the atmosphere and ocean waves as described in Süld et al. (2015) and Rasheed et al. (2017). The Charnock parameter [Eq. (4)] is passed from WW3 to HARMONIE-AROME. HARMONIE-AROME uses the wave-dependent Charnock parameter to calculate the surface roughness length [Eq. (3)] within the COARE3.0 scheme. The surface roughness length is then used in the calculation of the drag coefficient for momentum under neutral conditions [Eq. (2)] and thus influences the surface stress [Eq. (1)] and near surface winds. Thus, the 10-m wind speed is directly influenced by the updated surface roughness while other surface fluxes (e.g., turbulent fluxes of moisture and heat) are indirectly influenced through the modified wind speed. HARMONIE-AROME then passes the 10-m zonal and meridional wind components (as well as sea ice concentration and sea ice thickness) to WW3. WW3 uses the atmospheric forcing to estimate total and wave induced stress which are used to update the Charnock parameter. A schematic of this momentum coupling strategy is shown in Fig. 1. This
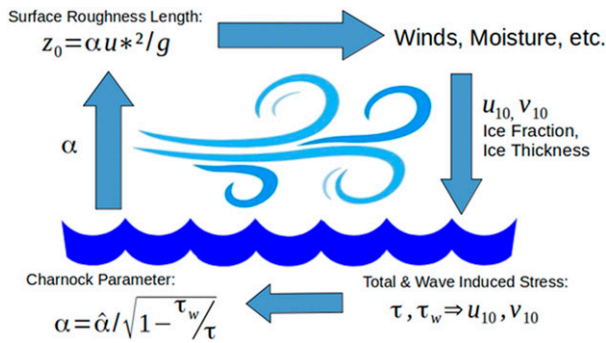
FIG. 1. Diagram of the momentum coupling between HARMONIE-AROME and WAVEWATCH III. For a description of the coupling strategy see the text. This figure has been adapted from the one seen in Süld et al. (2015) and Rasheed et al. (2017).

figure is adapted from the one seen in Süld et al. (2015) and Rasheed et al. (2017).

In the current study we use a 1-min time step for HARMONIE-AROME and a 5-min global time step for WW3. The coupling frequency in this framework is 30 min. During coupling time steps, fields are exchanged between HARMONIE-AROME and WW3. However, in order to avoid a deadlock in the OASIS coupler, we introduced a coupling lag of one model time step (i.e., 5 min) for the information being passed from WW3 to HARMONIE-AROME. In other words, HARMONIE-AROME uses the Charnock parameter from the previous WW3 time step to calculate the ocean surface roughness.

3. Experimental setup and methodology

We ran two simulations with the coupled forecast model over the time period between 6 December 2019 and 20 January 2020. These two simulations are: a "fully coupled" model simulation (two way coupling), and an "uncoupled" simulation (where the atmospheric model forces the wave model, but the wave model does not provide the Charnock parameter back to HARMONIE-AROME). The first two weeks of each experiment (6–19 December 2019) are considered the model "spinup" period to allow the wave field to fully adjust to the atmospheric forcing and allow waves from the lateral boundaries to fully propagate through the model domain. During the spinup period the forecast models are run with 3-h forecasts and 3-h cycling (meaning a 3-h forecast is initialized, complete with surface and atmospheric data assimilation, every three hours at 0000, 0300, 0600, 1200, 1500, 1800, and 2100 UTC). Once the spinup period is complete, the forecast model continues to run with 3-h cycling; however, 48 h forecasts are initialized at 0000 and 1200 UTC, with 3-h forecasts at all intermediate initialization times. The results herein only use output from the 48 h forecasts after the model has fully spun up (20 December 2019–20 January 2020).

To evaluate the accuracy of the coupled model we compare the coupled and uncoupled model simulations with satellite-based observations of 10-m wind speed and significant wave height H_s.

The 10-m wind speed from the "fully coupled" and "uncoupled" experiments is validated against satellite-based

Advanced Scatterometer (ASCAT) *MetOp-A* 12.5-km coastal 10-m wind speed product (OSI SAF/EARS Winds Team 2019). The model wind speed was additionally validated using coastal 12.5-km ASCAT products from *MetOp-B* and *MetOp-C* satellites. Although, since the conclusions remain unchanged, we only discuss the results from the comparison against ASCAT *MetOp-A* in the present paper.

First, we must regrid the higher resolution model data onto the same 12.5-km grid as the ASCAT winds to ensure a consistent comparison between the model and ASCAT wind speeds. Only collocated values in both time and space are compared. Collocated values are determined based on the availability of ASCAT observations given a specific time and spatial location.

For the wave verification, we use datasets provided by the Copernicus Marine Environmental Monitoring Service from five different satellite altimeters (*Jason-3*, *Sentinel-3A*, *Sentinel-3B*, *SARAL*/AltiKa, and *HaiYang-2B*) for validating H_s. The provider (see acknowledgments section for altimeter data availability) ensures that each along track H_s time series undergoes quality control and filtering. The collocation method is described in detail in Bohlinger et al. (2019), where the applied time and spatial constraints are 30 min and 6 km, respectively.

4. Results

To determine the overall effect of introducing wave coupling to a high resolution limited area weather forecast model, we analyze the difference in the overall mean values of 10-m wind speed, H_s, and the Charnock parameter of all forecasts during the entire one-month experiment from the two model simulations. The difference in overall mean values plotted in Fig. 2 are calculated as follows: the average of each 48-h forecast during the month-long experimental time period is taken (for all lead times from +0 to +48 h). The mean across all forecasts is then calculated and the uncoupled result is subtracted from the fully coupled result.

Figure 2 clearly shows that the introduction of two-way coupling with a wave model reduces the average wind speed of the forecast over open water. Additionally, the average significant wave height is also reduced. An increase in surface roughness (as suggested by the increase in the magnitude of the Charnock parameter) is consistent with the simulated decreased 10-m wind speed and decreased significant wave height (Fig. 2). These results agree with the findings of Wu et al. (2019). The effect wave coupling has on the surface roughness, wind speed, and wave height is physically consistent and provides intrinsic scientific value as the mean impact of the wave coupling in Fig. 2 confirms the expected theoretical impact of wave coupling through momentum [Eqs. (1)–(4)] thus supporting the validity of wave coupling with this model configuration in an Arctic region.

A storm approaching the coast of Norway on 3 January 2020 is selected as a case study to demonstrate the type of severe weather conditions common in this region. We also use this case study to further assess the coupled model capability to accurately represent extreme weather events.
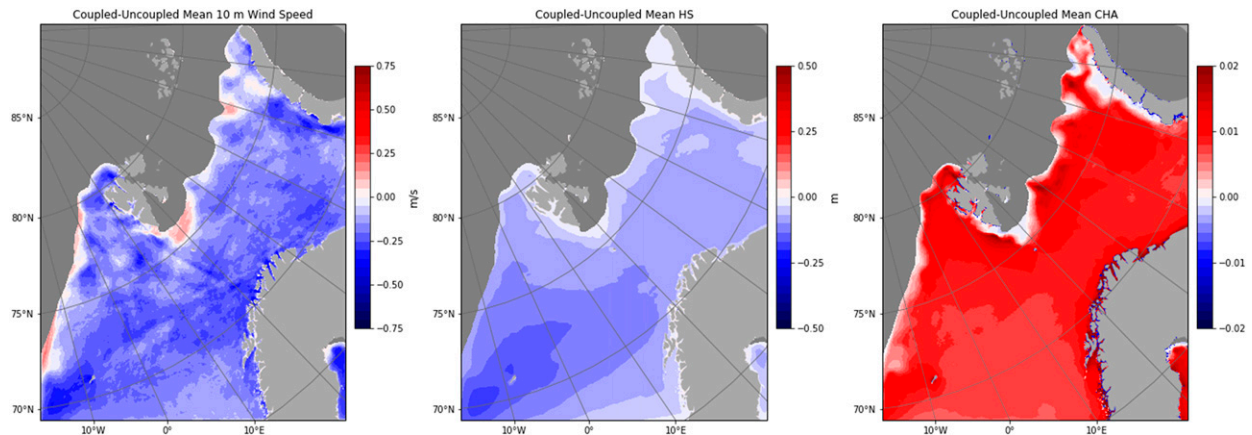
FIG. 2. The difference between the mean coupled and mean uncoupled response for (left) 10-m wind speed, (middle) significant wave height, and (right) Charnock parameter. The region covered by sea ice, defined as the area with a mean sea ice concentration greater than 50%, is masked out in dark gray shading. The means are the 0–48-h forecast means (the average across all lead time from 0 to 48 h for each forecast), which are then averaged together.

Figure 3 shows both observed and modeled values of 10-m wind speed and H_s valid on 3 January 2020. The two left panels contain all satellite overpasses through the domain between 1100 and 1500 UTC 3 January 2020. In comparison, the middle and right panels show the coupled and uncoupled model output valid at 1100 UTC 3 January 2020. This figure illustrates the spatial coverage of the satellite-based 10-m wind speed and HS observations, as well as demonstrates the capability of the model to simulate a high impact weather event.

Next, the mean sea level pressure and 10-m wind speed from the two model runs are compared against land-based station observations between 0000 UTC 2 January 2020 and 1200 UTC 5 January 2020. Three coastal stations whose elevation is close to sea level are selected: Jan Mayen, Bjørnøya, and Bø i Vesterålen III in the Lofoten archipelago in Norway. The locations of the selected stations are shown in the left panel of Fig. 4. The forecast coupled and uncoupled model pressure and wind speed plotted are the values from the single grid cell closest to the station location. Time series for observed surface pressure and model adjusted mean sea level pressure are shown in the top right while observed surface wind speed and model 10-m wind speed are shown in the bottom right panels. The continuous time series for forecast wind speed and surface pressure is constructed from the forecasts at lead times from +0 to +11 h from the forecasts initialized at 0000 and 1200 UTC. The passing of the storm (as seen in the mean sea level pressure field of Fig. 3) is evidenced by the pressure minima and high wind speeds (Fig. 4) between 2 and 3 January at these stations.

The difference in the mean sea level pressure between the coupled and uncoupled model at the selected stations is negligible; however, there are several instances where the coupled model more closely represents the observed wind speed characteristics than the uncoupled model (Fig. 4). For example, the coupled model outperforms the uncoupled model in the Lofoten station (shown in red) during the approach and landfall of the storm in question (between

1200 UTC 3 January and 0000 UTC 4 January). Additionally, the coupled model closely matches the observed wind speeds and consistently outperforms the uncoupled model during case study time period at the station of Bjørnøya (shown in green).

To quantify the improvement at these stations in the coupled model 10-m wind speed during this case study, we calculate the coupled and uncoupled model bias, mean absolute error (mae), and standard deviation of the errors (estd) for each of the three stations. The results are reported in Table 1. During this 48-h time period, the coupled model outperforms the uncoupled model as evidenced by the smaller error statistics (for all three metrics) at all the locations.

Figure 5 shows scatterplots comparing collocated (in both time and space) 10-m wind speed forecast from the atmospheric model output against ASCAT-A data for the coupled and uncoupled model experiments. The total number of individual pairs of collocated wind speed values for all forecasts at forecast initialization times (lead time +0 h) is approximately 100 000. To quantify the general relationship between observations and the model simulations for a given wind speed, we calculate the wind speed for percentiles from 0 to 100 (in increments of 1%) for the ASCAT data and plot it against the wind speed percentiles of the coupled and uncoupled model data, where the zeroth percentile corresponds to the minimum wind speed, the 50th percentile corresponds to the median, and the 100th percentile corresponds to the maximum wind speed.

The scatterplots in Fig. 5 show strong agreement between the modeled and ASCAT wind speeds with majority of the values lying close to the diagonal (black solid line; Fig. 5). Both coupled and uncoupled model forecast winds are highly correlated with ASCAT-A wind speeds with a correlation coefficient of 0.92. The scatterplots show the coupled model wind speed more closely match the observed ASCAT winds speeds at values greater than $20\,\mathrm{m\,s}^{-1}$. This is evident in the wind speed percentile lines which show the coupled model lies closer to the diagonal than the uncoupled model at high wind speeds.
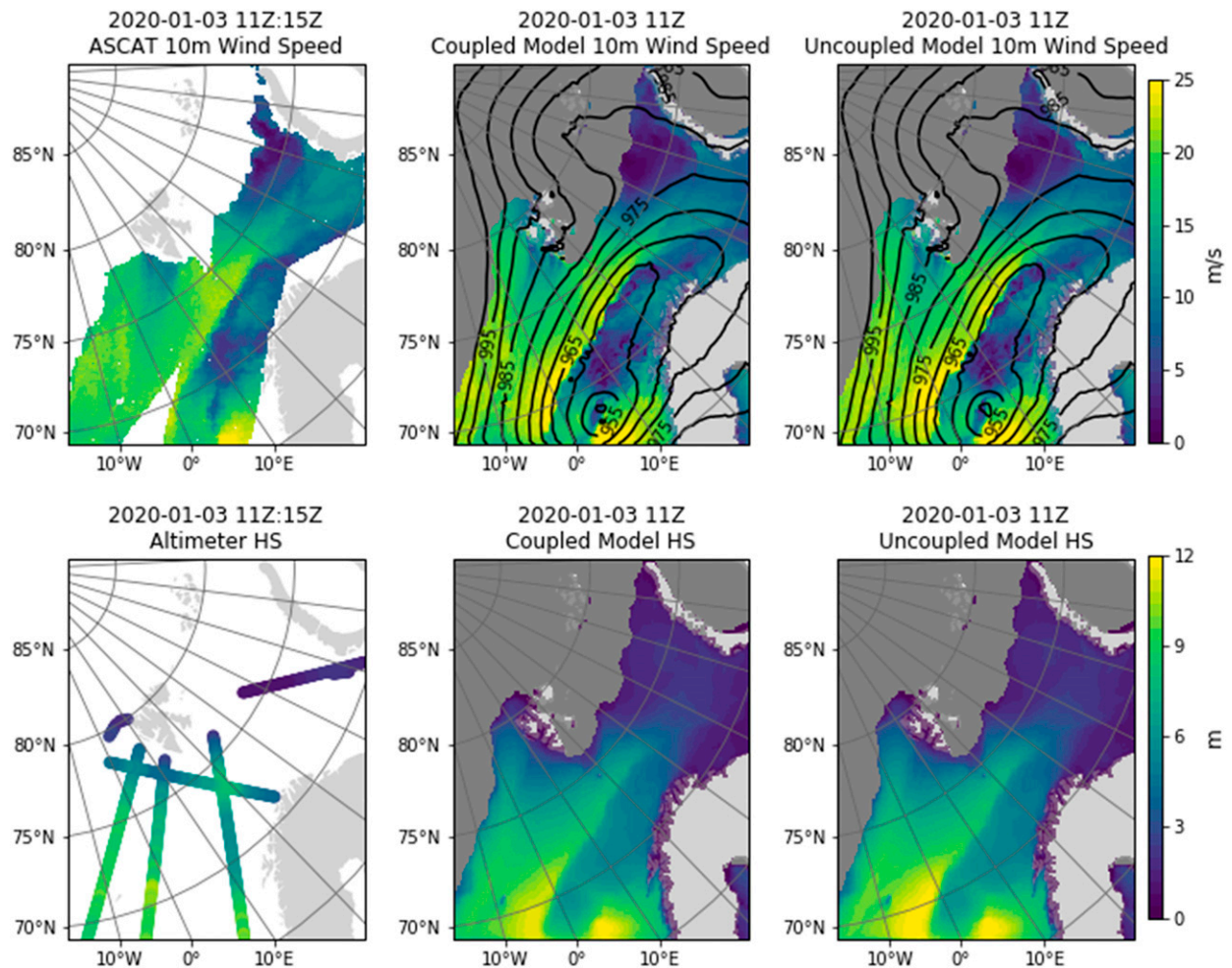
FIG. 3. Case study of a storm approaching the coast of Norway in early January 2020. (top left) The 10-m wind speed ASCAT *MetOp-A* overpasses through the AROME-Arctic domain between 1100 and 1500 UTC 3 Jan 2020. (top center) The coupled and (top right) the uncoupled model 10-m wind speed (shading) and mean sea level pressure (black contours) valid at 1100 UTC 3 Jan 2020. (bottom left) The satellite altimeter significant wave height overpasses through the domain between 1100 and 1500 UTC 3 Jan 2020. (bottom center) The coupled and (bottom right) the uncoupled model significant wave height valid at 1100 UTC 3 Jan 2020.

We only show scatterplots valid at the forecast initialization time (lead time of +0 h) in Fig. 5; however, we repeat this scatterplot analysis at forecast lead times of +12, +24, +36, and +48 h in order to calculate the statistic metrics as a function of lead time to further assess the coupled model performance. At each lead time we calculate the coupled and uncoupled model bias, estd, and correlation against ASCAT-A 10-m wind speed.

Figure 6 shows the 10-m wind speed bias, estd, and correlation as a function of forecast lead time (from +0 to +48 h). The bias of the fully coupled model is larger in magnitude than the bias of the uncoupled model (Fig. 6); however, the coupled model estd shows slightly smaller values than the uncoupled model, indicating the coupled model contains less variability with respect to the satellite observations than the uncoupled model. The estd for both the coupled and uncoupled experiments increase with the forecast lead time while the correlation with ASCAT wind speed decreases with forecast lead time for

both experiments. This is expected as forecast model states slowly diverge from reality with time.

To determine the specific impact of wave coupling at different wind speeds, Fig. 7 shows the coupled and uncoupled model estd for the following observed wind speed categories: 5–10, 10–15, 15–20, and 20–25 m s^{-1} as a function of forecast lead time. The results show that the coupled model has smaller error standard deviations than the uncoupled model for all wind speed categories. However, the greatest improvement due to coupling clearly occurs for wind speeds greater than 20 m s^{-1} at forecast lead times less than 36 h.

Additionally, we calculate the forecast mean error metrics (calculated as the mean over forecast lead times from +0 to +48 h) for each wind speed category and summarize the values in Table 2. The mean bias of the coupled model is larger than the uncoupled model for all wind speeds; however, the coupled model mean estd is smaller for all wind speeds. The largest improvement in estd occurs for the highest wind speed
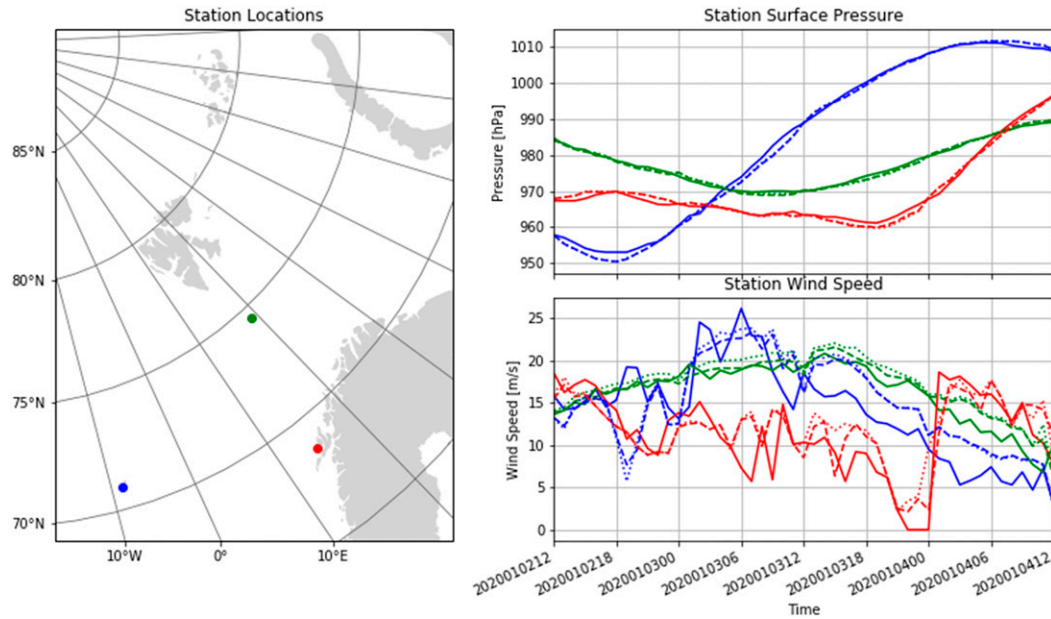
FIG. 4. (left) The location of three selected land-based observation stations: Jan Mayen (blue), Bjørnøya (green), and Bø i Vesterålen III in the Lofoten archipelago (red). Time series of (top right) surface pressure and (bottom right) wind speed at each of the station locations between 1200 UTC 2 Jan 2020 and 1200 UTC 4 Jan 2020. Station measurements show the observed surface pressure and surface wind speed, while the corresponding coupled and uncoupled model data show adjusted mean sea level pressure and 10-m wind speed. The line colors in the panels on the right correspond to the station color plotted in the left panel. Solid lines indicate the observed values and dashed (dotted) lines show coupled (uncoupled) model output from the single model grid cell closest to station location.

category (20–25 m s^{-1}). Overall, wave coupling provides the greatest improvements at winds speeds over 15 m s^{-1} as evidenced by the decreased mae and estd values.

Next, we compare model significant wave height H_s against satellite-based observations. Figure 8 shows scatterplots comparing collocated values of significant wave height from satellite altimeter data against coupled and uncoupled model forecasts. Only the scatterplots valid at the forecast initialization (lead time of +0 h) are shown. Similar to the wind speed analysis, we calculate the significant wave height for percentiles from 0 to 100 (in increments of 1%) from the altimeter data and plot it against the significant wave height percentiles of the coupled and uncoupled model data.

Figure 8 shows very good agreement between the collocated values of model and satellite-based significant wave height at the forecast initialization time. Both coupled and uncoupled model H_s are highly correlated with satellite-based altimeter data with a correlation coefficient value of 0.97. The H_s estd of the coupled model is slightly lower than the estd of the uncoupled model at lead time of +0 h. The figure shows that the coupled model H_s more closely matches the observed H_s at values greater than 6 m. This is evident in the percentile lines which show that the coupled model's H_s lies closer to the diagonal at values greater than 6 m than that of the uncoupled model. This indicates that the greatest improvement due to coupling of atmosphere and waves occurs when the significant wave height is large.

We next compare the modeled significant wave height against satellite-based observations as a function of forecast

lead time for forecast lead times of +0, +12, +24, +36, and +48 h (see the Fig. 9). Figure 9 shows larger magnitude bias in the coupled model H_s which is consistent with the larger bias seen in the coupled 10-m wind speed results (Fig. 6). Although the bias is larger for the coupled model, the estd of the coupled model H_s is smaller than the uncoupled model estd. Similarly to the wind speed results, this suggests that although wave coupling increases the overall model bias of H_s, it reduces the error variability or increases the model precision of H_s. Furthermore, Fig. 8 shows that the correlation of coupled model against satellite-based H_s is higher than the correlation of the uncoupled model. Similar to the 10-m wind speed results, both coupled and uncoupled model H_s results show increasing estd values and decreasing correlations as forecast lead time

TABLE 1. Bias, mae, and estd for 10-m wind speeds at selected land-based observation stations. Error metrics are calculated for the 10-m wind speed data between 1200 UTC 2 Jan 2020 and 1200 UTC 4 Jan 2020 (corresponding to Fig. 4).

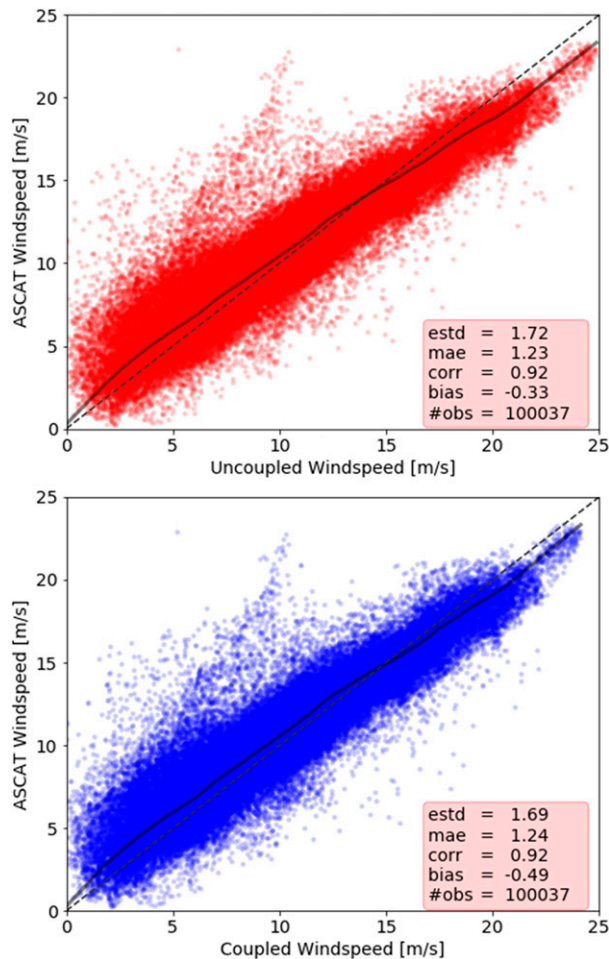|	Jan Mayen	Bjørnøya	Bø i Vesterålen
Uncoupled bias	1.15	1.22	0.83
Coupled bias	0.93	0.64	0.38
Uncoupled mae	2.99	1.45	2.36
Coupled mae	2.88	1.01	2.27
Uncoupled estd	3.65	1.27	3.14
Coupled estd	3.51	1.22	2.92

FIG. 5. Scatterplots comparing collocated (in both time and space) 10-m wind speed from model output against ASCAT *MetOp-A* data. Only values valid at forecast initialization times (forecast lead time of +0 h) are shown. (top) 10-m wind speed of ASCAT plotted against the 10-m wind speed estimated by the uncoupled model forecasts. (bottom) The same comparison for ASCAT wind speed plotted against the fully coupled model wind speed. The dark gray lines show the ASCAT percentiles plotted against the coupled and uncoupled model wind speed percentiles (see text for more details). The black dashed line shows the diagonal for reference.

increases. However, the estd of the coupled model grows at a slower rate than the uncoupled estd.

The mean error metrics (calculated as the mean for forecast lead times from +0 to +48 h) for significant wave height categories are summarized in Table 3. Similar to the mean bias for wave height categories less than 6 m is larger in the coupled model, however, the mean bias for coupled model is slightly smaller for the largest wave categories (greater than 6 m). The estd and mae for the coupled and uncoupled models are of similar magnitude across all wave height categories except for waves over 9 m in height, which shows the coupled model contains smaller estd and mae values than the uncoupled model. Similar to the 10-m wind speed conclusions, the largest
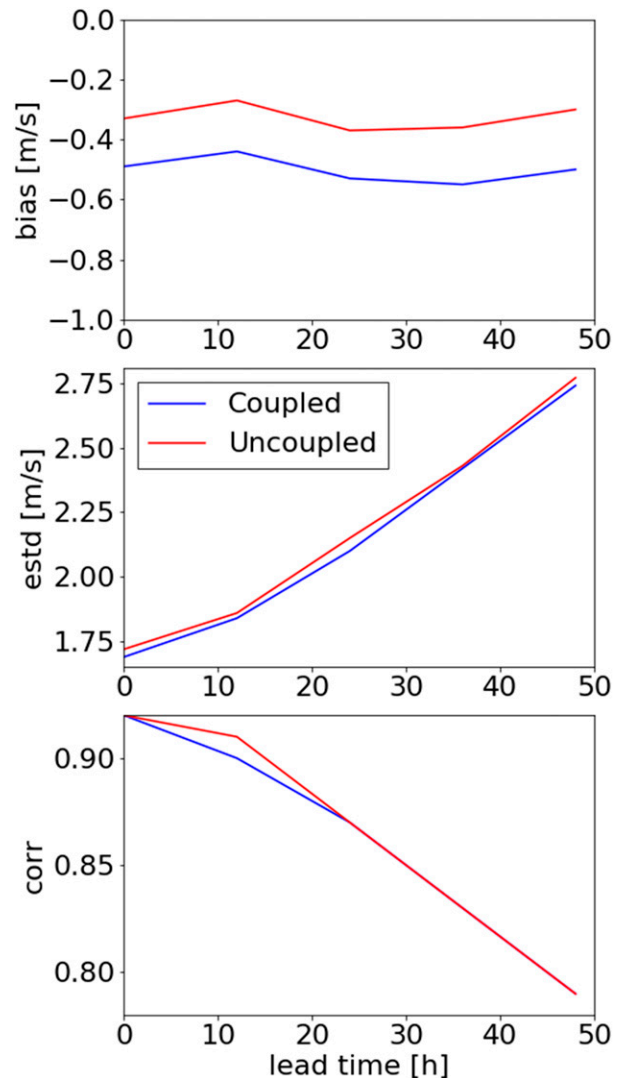

FIG. 6. (top) The 10-m wind speed bias, (middle) standard deviation of errors (estd), and (bottom) correlation of the uncoupled and coupled model forecasts as a function of forecast lead times between +0 and +48 h.

improvements due to wave coupling occur for the largest wave heights (waves over 6 m in height).

5. Discussion and conclusions

This paper describes a newly developed, high resolution, regional forecasting system that couples an atmospheric forecast model to a spectral wave model as the first step toward a fully coupled Arctic forecasting system. This coupled forecasting system uses the HARMONIE-AROME configuration of the ALADIN-HIRLAM NWP system for the atmospheric model, WAVEWATCH III for the wave model, and the OASIS3-MCT coupler. The coupling process is organized as follows: the 10-m zonal and meridional wind components, as well as sea ice fraction and sea ice thickness,
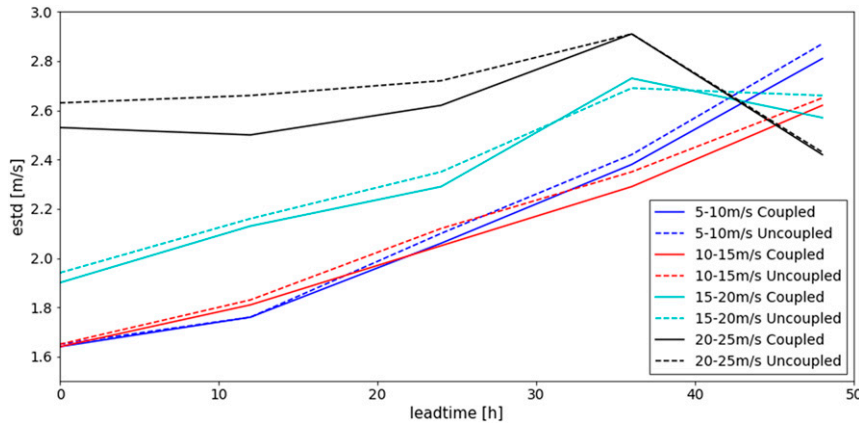
FIG. 7. The 10-m wind speed standard deviation of errors (estd) in the coupled and uncoupled model forecasts for distinct wind speed categories as a function of forecast lead times between +0 and +48 h.

are passed from HARMONIE-AROME to WAVEWATCH III. WAVEWATCH III determines the full spectral wave response to the atmospheric forcing and calculates the Charnock parameter. The Charnock parameter is then passed back to HARMONIE-AROME in order to update the surface roughness in the surface parameterization package. The updated surface roughness ultimately modifies the near-surface winds thus closing the coupling cycle.

The mean response of the model 10-m wind speed, H_s, and Charnock parameter over the one month experimental time frame indicates that introducing wave coupling to the convection-resolving Arctic forecast model generates a physically consistent response between the atmosphere and wave systems thus confirming theory holds true with our model configuration in this region.

For the verification of the newly developed atmosphere–wave coupled forecast model, model forecasts were compared against satellite-based observations and several land-based station observations. We compared the model 10-m wind speed against 10-m wind speed from satellite scatterometer and the model significant wave height against significant wave height from satellite-based altimeter data as well as comparing model wind speed against near-surface wind speed observations from coastal observation stations. The model forecasts from both the coupled and uncoupled experiments are highly correlated with the satellite and land based observations (Figs. 3–6), meaning, the addition of wave coupling does not

degrade the quality of our numerical weather prediction system. Additionally, we find several instances where the coupled model wind speed more closely matches station observations and contains smaller errors than the uncoupled model as evidenced during the approach and landfall of a storm in early January 2020 (Fig. 4, Table 1).

The model slightly underestimates wind speeds below $15 \, \mathrm{m \, s^{-1}}$ and wave heights less than 6 m (Figs. 5 and 8, Tables 2 and 3). Considering the introduction of wave coupling to the forecast system further reduces the wind speed and significant wave height, we see an increase in the magnitude of the mean negative bias for 10-m winds and H_s. The introduction of remote sensing data assimilation in the forecasts may improve the bias and will be tested in future work. Furthermore, the fully coupled experiment has smaller error standard deviation values than the uncoupled experiment for both 10-m wind speed and H_s indicating that wave coupling reduces the error variability of wind speeds and significant wave height forecasts.

Decreased error variability suggests that wave coupling improves the overall forecast precision of 10-m wind speed and significant wave height, a benefit that persists with increasing forecast lead time. Furthermore, we show that including wave coupling provides the greatest improvement on the short-term forecast precision when 10-m wind speeds exceed $20 \, \mathrm{m \, s^{-1}}$ and significant wave heights are greater than 6 m.

Cumulatively, the results presented in this study show that coupling HARMONIE-AROME to WAVEWATCH III is

TABLE 2. Average bias, mae, and estd for 10-m wind speed categories. Each error statistic is calculated as the average of forecast lead times from +0 to +48 h.

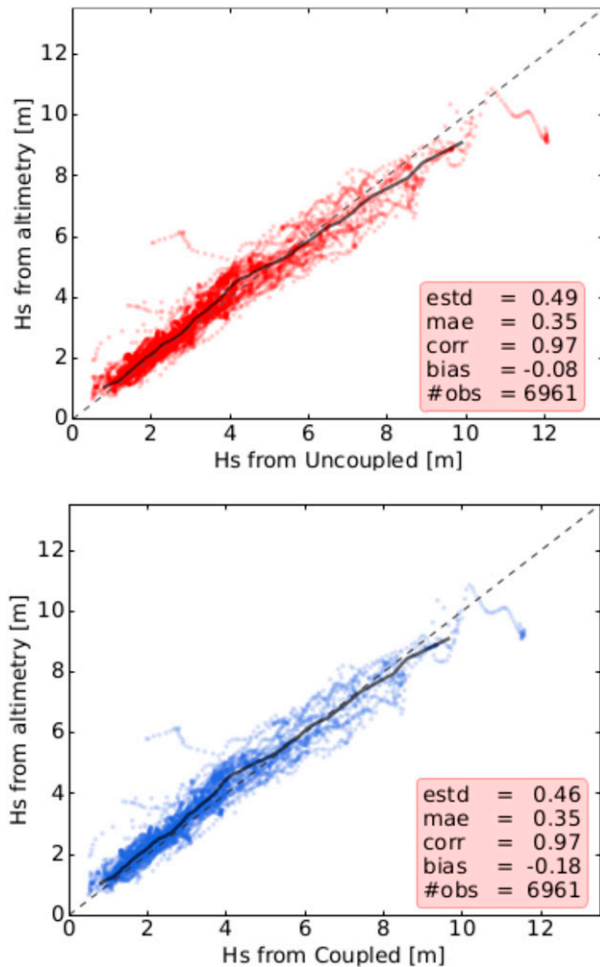|	5–10 m s^{-1}	10–15 m s^{-1}	15–20 m s^{-1}	20–25 m s^{-1}
Uncoupled bias	−0.51	−0.45	−0.04	−0.05
Coupled bias	−0.60	−0.67	−0.41	−0.63
Uncoupled mae	1.59	1.59	1.76	2.19
Coupled mae	1.59	1.60	1.70	1.98
Uncoupled estd	2.06	2.22	2.59	3.15
Coupled estd	2.04	2.18	2.55	3.06

FIG. 8. Scatterplots comparing collocated values of significant wave height from satellite altimeter data against (top) uncoupled and (bottom) coupled model forecasts. Only collocated points at all forecast initialization times (forecast lead time of +0 h) are shown. The dark gray lines show the altimeter H_s for percentiles from 0% to 100% plotted against the H_s coupled and uncoupled model percentiles (see text for more details). The black dashed line shows the diagonal for reference.

beneficial to kilometer-scale numerical weather prediction in our Arctic domain. Coupled forecasting is important in Arctic regions like the one used in this study due to the occurrence of strong wind–wave interactions. Although the results herein show wave coupling reduces model variability of 10-m wind speed and significant wave height in short-term forecasts, especially during high wind and wave conditions, further work is required to determine the exact impact of wave coupling on forecast quality during the most extreme Arctic weather events such as polar lows. Additional process-based case studies would be beneficial; however, due to the high computational cost of running this coupled forecasting system (which is approximately 1.5 times more costly than the reference configuration of HARMONIE-AROME) it was impractical to run a large number of experiments at this time.
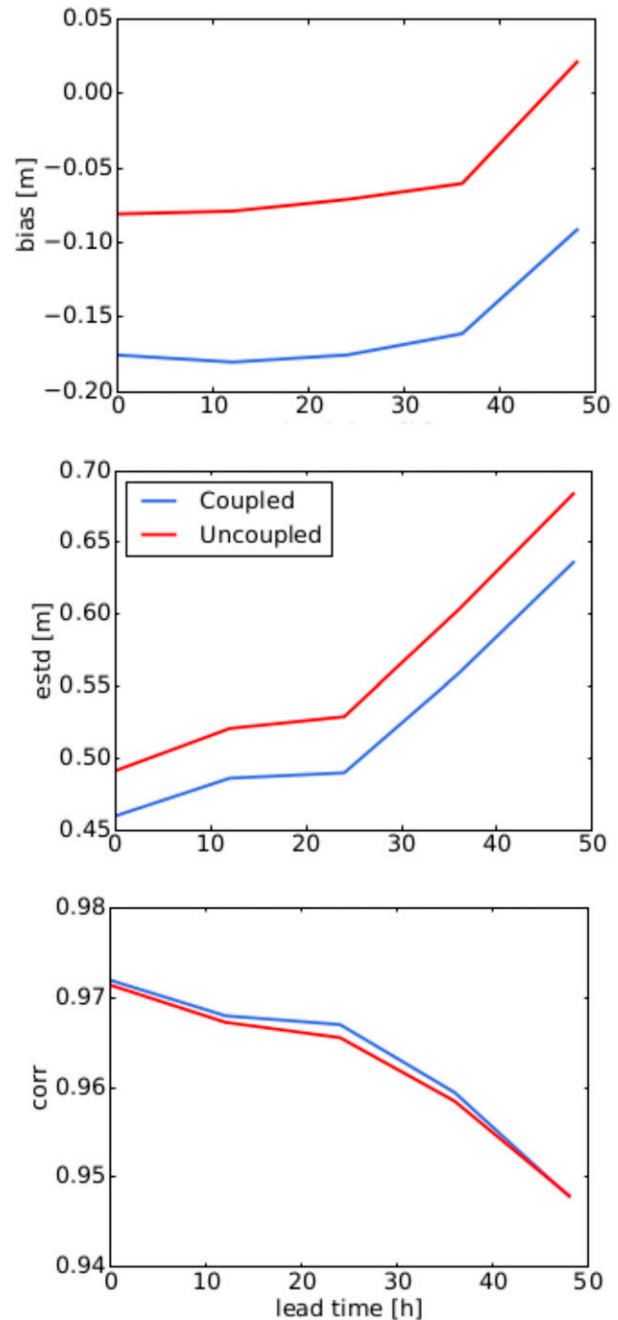

FIG. 9. (top) The significant wave height bias, (middle) standard deviation of errors (estd), and (bottom) correlation of the coupled and uncoupled model forecasts as a function of forecast lead times between +0 and +48 h.

Many areas of our coupled numerical weather prediction system require further improvements. For example, the ST3 wave physics of WW3, used in the present study, show a considerable sensitivity to swell conditions (WAVEWATCH III Development Group 2016). Although a more advanced physics package may perform better in certain situations, the higher computational costs and desire to match the physics settings to

TABLE 3. Average bias, mae, and estd statistics for significant wave height categories. Each mean error statistic is calculated as the average of forecast lead times from +0 to +48 h.

	0.5–3 m	3–6 m	6–9 m	9+ m
Uncoupled bias	−0.11	−0.11	0.33	1.52
Coupled bias	−0.16	−0.21	0.13	1.11
Uncoupled mae	0.23	0.38	0.59	1.59
Coupled mae	0.25	0.40	0.52	1.24
Uncoupled estd	0.28	0.47	0.64	1.23
Coupled estd	0.28	0.46	0.62	1.11

those used in the current operational model made them impractical for this study.

Additionally, we recognize some limitations in validating our coupled forecast model performance against satellite products. ASCAT 10-m wind speed estimates are known to have biases at both high and low wind speed extremes. Additionally, we realize there is an inability to analyze the kilometer-scale wind speed variability in the coupled model due to the coarser resolution of the ASCAT data; however, the quantity of high resolution wind speed observations over open ocean is limited. This introduces challenges to accurately validate model performance, particularly during the highest wind conditions when it appears the greatest benefit of wave coupling occurs. However, we select ASCAT data for the wind speed validation due to its good spatial and temporal coverage as well as the lack of in situ wind and wave observations over open ocean.

The coupling of kilometer-scale forecasting systems for the Arctic provides many challenges. Capturing the complex interactions between wind, waves, and sea ice is critical to estimating surface fluxes and thus crucial for producing more accurate forecasts. This is especially true in Arctic regions where these interactions can play a large role on the development of weather.

The wave coupling development described in this study, which explicitly captures the interactions between the atmosphere and ocean waves, is only one step toward developing a fully coupled numerical weather, wave, sea ice, and ocean prediction system. Coupling efforts need to continue in order to further advance high latitude short-term forecasting capabilities. One example of such an effort is to introduce a full sea ice model into our atmosphere–wave forecasting system. Explicitly representing the interactions between atmosphere, waves and sea ice, could improve forecasts in areas surrounding the marginal ice zone where complex wave-ice–atmosphere interactions occur (Boutin et al. 2019; Montiel and Squire 2017; Løken et al. 2020; Elvidge et al. 2016) and changes in the small scale structure of the sea ice can have a far reaching impact on the weather forecasts (Batrak and Müller 2018).

Finally, we would like to stress that modeling work, while being invaluable toward understanding the coupled Earth system, is insufficient by itself and more observations representing atmosphere–wave–sea ice interactions in polar regions are desperately needed to guide model development efforts such as those presented herein.

APPENDIX

Complete List of WW3 Settings Used in Coupled Framework

The list of settings is as follows: F90 NOGRB NOPA LRB4 NC4 TRKNC DIST MPI PR3 UQ FLX0 LN1 ST3 STAB0 NL1 BT4 DB1 MLIM TR0 BS0 IC2 IS0 REF1 XX0 WNT0 WNX1 RWND CRT1 CRX1 TIDE COU OASIS OASACM O0 O1 O2 O2a O2b O2c O3 O4 O5 O6 O7.

REFERENCES

Ardhuin, F., F. Collard, B. Chapron, F. Girard-Ardhuin, G. Guitton, A. Mouche, and J. E. Stopa, 2015: Estimates of ocean wave heights and attenuation in sea ice using the SAR wave mode on Sentinel-1A. *Geophys. Res. Lett.*, **42**, 2317–2325, https://doi.org/10.1002/2014GL062940.

Batrak, Y., and M. Müller, 2018: Atmospheric response to kilometer-scale changes in sea ice concentration within the marginal ice zone. *Geophys. Res. Lett.*, **45**, 6702–6709, https://doi.org/10.1029/2018GL078295.

——, E. Kourzeneva, and M. Homleid, 2018: Implementation of a simple thermodynamic sea ice scheme, SICE version 1.0-38h1, within the ALADIN-HIRLAM numerical weather prediction system version 38h1. *Geosci. Model Dev.*, **11**, 3347–3368, https://doi.org/10.5194/gmd-11-3347-2018.

Bengtsson, L., and Coauthors, 2017: The HARMONIE-AROME model configuration in the ALADIN-HIRLAM NWP system. *Mon. Wea. Rev.*, **145**, 1919–1935, https://doi.org/10.1175/MWR-D-16-0417.1.

Bohlinger, P., Ø. Breivik, T. Economou, and M. Müller, 2019: A novel approach to computing super observations for probabilistic wave model validation. *Ocean Modell.*, **139**, 101404, https://doi.org/10.1016/j.ocemod.2019.101404.

Boutin, G., C. Lique, F. Ardhuin, C. Rousset, C. Talandier, M. Accensi, and F. Girard-Ardhuin, 2019: Towards a coupled model to investigate wave–sea ice interactions in the Arctic

marginal ice zone. *Cryosphere*, **14**, 709–735, https://doi.org/10.5194/tc-14-709-2020.

Breivik, Ø., K. Mogensen, J.-R. Bidlot, M. A. Balmaseda, and P. A. E. M. Janssen, 2015: Surface wave effects in the NEMO ocean model: Forced and coupled experiments. *J. Geophys. Res. Oceans*, **120**, 2973–2992, https://doi.org/10.1002/2014JC010565.

Cavalieri, D. J., and C. L. Parkinson, 2012: Arctic sea ice variability and trends, 1979–2010. *Cryosphere*, **6**, 881–889, https://doi.org/10.5194/tc-6-881-2012.

Chen, S. S., W. Zhao, M. A. Donelan, and H. L. Tolman, 2013: Directional wind–wave coupling in fully coupled atmosphere–wave–ocean models: Results from CBLAST-Hurricane. *J. Atmos. Sci.*, **70**, 3198–3215, https://doi.org/10.1175/JAS-D-12-0157.1.

Comiso, J. C., and D. K. Hall, 2014: Climate trends in the Arctic as observed from space. *Wiley Interdiscip. Rev.: Climate Change*, **5**, 389–409, https://doi.org/10.1002/wcc.277.

Dawson, J., W. Hoke, M. Lamers, D. Liggett, G. Ljubicic, B. Mills, E. Stewart, and R. Thoman, 2017: Navigating weather, water, ice and climate information for safe polar mobilities. Tech. Rep. WWRP/PPP 5, WMO, 74 pp., https://epic.awi.de/id/eprint/46211/.

Elvidge, A. D., I. A. Renfrew, A. I. Weiss, I. M. Brooks, T. A. Lachlan-Cope, and J. C. King, 2016: Observations of surface momentum exchange over the marginal ice zone and recommendations for its parametrisation. *Atmos. Chem. Phys.*, **16**, 1545–1563, https://doi.org/10.5194/acp-16-1545-2016.

Fairall, C. W., E. F. Bradley, J. E. Hare, A. A. Grachev, and J. B. Edson, 2003: Bulk parameterization of air–sea fluxes: Updates and verification for the COARE algorithm. *J. Climate*, **16**, 571–591, https://doi.org/10.1175/1520-0442(2003)016<0571:BPOASF>2.0.CO;2.

GEBCO Bathymetric Compilation Group, 2020: The GEBCO 2020 Grid—A continuous terrain model of the global oceans and land. British Oceanographic Data Centre, National Oceanography Centre, NERC, United Kingdom, accessed 25 October 2019, https://doi.org/10.5285/a29c5465-b138-234d-e053-6c86abc040b9.

Hall, C. M., and J. Saarinen, 2010: Polar tourism: Definitions and dimensions. *Scand. J. Hospitality Tourism*, **10**, 448–467, https://doi.org/10.1080/15022250.2010.521686.

Hansen, J., R. Ruedy, M. Sato, and K. Lo, 2010: Global surface temperature change. *Rev. Geophys.*, **48**, RG4004, https://doi.org/10.1029/2010RG000345.

Hanssen-Bauer, I., and Coauthors, 2018: Climate in Svalbard 2100 editors—A knowledge base for climate adaptation. NCCS Rep. 1/2019, 207 pp.

Huang, J., and Coauthors, 2017: Recently amplified arctic warming has contributed to a continual global warming trend. *Nat. Climate Change*, **7**, 875–879, https://doi.org/10.1038/s41558-017-0009-5.

Isachsen, P. E., M. Drivdal, S. Eastwood, Y. Gusdal, G. Noer, and O. Saetra, 2013: Observations of the ocean response to cold air outbreaks and polar lows over the Nordic Seas. *Geophys. Res. Lett.*, **40**, 3667–3671, https://doi.org/10.1002/grl.50705.

Janssen, P. A. E. M., 1982: Quasilinear approximation for the spectrum of wind-generated water waves. *J. Fluid Mech.*, **117**, 493–506, https://doi.org/10.1017/S0022112082001736.

——, 1991: Quasi-linear theory of wind-wave generation applied to wave forecasting. *J. Phys. Oceanogr.*, **21**, 1631–1642, https://doi.org/10.1175/1520-0485(1991)021<1631:QLTOWW>2.0.CO;2.

——, 2004: The *Interaction* of *Ocean Waves* and *Wind*. Cambridge University Press, 308 pp.

Jung, T., and Coauthors, 2016: Advancing polar prediction capabilities on daily to seasonal time scales. *Bull. Amer. Meteor. Soc.*, **97**, 1631–1647, https://doi.org/10.1175/BAMS-D-14-00246.1.

Karl, T. R., and Coauthors, 2015: Possible artifacts of data biases in the recent global surface warming hiatus. *Science*, **348**, 1469–1472, https://doi.org/10.1126/science.aaa5632.

Kudryavtsev, V. N., V. K. Makin, and B. Chapron, 1999: Coupled sea surface-atmosphere model 2. Spectrum of short wind waves. *J. Geophys. Res.*, **104**, 7625–7639, https://doi.org/10.1029/1999JC900005.

Le Moigne, P., 2018: SURFEX scientific documentation. Accessed 27 April 2018, http://www.umr-cnrm.fr/surfex/.

Liu, A. K., and E. Mollo-Christensen, 1988: Wave propagation in a solid ice pack. *J. Phys. Oceanogr.*, **18**, 1702–1712, https://doi.org/10.1175/1520-0485(1988)018<1702:WPIASI>2.0.CO;2.

——, B. Holt, and P. W. Vachon, 1991: Wave propagation in the marginal ice zone: Model predictions and comparisons with buoy and synthetic aperture radar data. *J. Geophys. Res.*, **96**, 4605–4621, https://doi.org/10.1029/90JC02267.

Liu, B., H. Liu, L. Xie, C. Guan, and D. Zhao, 2011: A coupled atmosphere–wave–ocean modeling system: Simulation of the intensity of an idealized tropical cyclone. *Mon. Wea. Rev.*, **139**, 132–152, https://doi.org/10.1175/2010MWR3396.1.

Løken, T. K., J. Rabault, E. E. Thomas, M. Müller, K. H. Christensen, G. Sutherland, and A. Jensen, 2020: A comparison of wave observations in the Arctic marginal ice zone with spectral models. *25th IAHR Int. Symp. on Ice*, Trondheim, Norway, IAHR, https://doi.org/10.13140/RG.2.2.10185.90723.

Makin, V. K., and V. N. Kudryavtsev, 1999: Coupled sea surface-atmosphere model 1. Wind over waves coupling. *J. Geophys. Res.*, **104**, 7613–7623, https://doi.org/10.1029/1999JC900006.

Masson, V., and Coauthors, 2013: The SURFEXv7.2 land and ocean surface platform for coupled or offline simulation of earth surface variables and fluxes. *Geosci. Model Dev.*, **6**, 929–960, https://doi.org/10.5194/gmd-6-929-2013.

Meredith, M., and Coauthors, 2019: Polar regions. *IPCC Special Report on the Ocean and Cryosphere in a Changing Climate*, H.-O. Pörtner et al., Eds., IPCC, 203–320.

Miles, J. W., 1957: On the generation of surface waves by shear flows. *J. Fluid Mech.*, **3**, 185, https://doi.org/10.1017/S0022112057000567.

Montiel, F., and V. A. Squire, 2017: Modelling wave-induced sea ice break-up in the marginal ice zone. *Proc. Roy. Soc.*, **A473**, 20170258, https://doi.org/10.1098/rspa.2017.0258.

Müller, M., Y. Batrak, J. Kristiansen, M. A. Køltzow, G. Noer, and A. Korosov, 2017a: Characteristics of a convective-scale weather forecasting system for the European Arctic. *Mon. Wea. Rev.*, **145**, 4771–4787, https://doi.org/10.1175/MWR-D-17-0194.1.

——, and Coauthors, 2017b: AROME-MetCoOp: A Nordic convective-scale operational weather prediction model. *Wea. Forecasting*, **32**, 609–627, https://doi.org/10.1175/WAF-D-16-0099.1.

OSI SAF/EARS Winds Team, 2019: ASCAT Wind Product User Manual. EUMETSAT, 28 pp., https://scatterometer.knmi.nl/publications/pdf/ASCAT_Product_Manual.pdf.

Rasheed, A., J. K. Süld, M. Tabib, T. Kvamsdal, and J. Kristiansen, 2017: Demonstrating the impact of bidirectional coupling on the performance of an ocean-met model. *Energy Procedia*, **137**, 443–451, https://doi.org/10.1016/j.egypro.2017.10.368.

Ricchi, A., M. M. Miglietta, P. P. Falco, A. Benetazzo, D. Bonaldo, A. Bergamasco, M. Sclavo, and S. Carniel, 2016: On the use of a coupled ocean-atmosphere-wave model during an extreme cold air outbreak over the Adriatic Sea. *Atmos. Res.*, **172–173**, 48–65, https://doi.org/10.1016/j.atmosres.2015.12.023.

Smith, L. C., and S. R. Stephenson, 2013: New Trans-Arctic shipping routes navigable by midcentury. *Proc. Natl. Acad. Sci. USA*, **110**, E1191–E1195, https://doi.org/10.1073/pnas.1214212110.

Stocker, A. N., A. H. Renner, and M. Knol-Kauffman, 2020: Sea ice variability and maritime activity around Svalbard in the period 2012–2019. *Sci. Rep.*, **10**, 17043, https://doi.org/10.1038/s41598-020-74064-2.

Stoll, P. J., T. M. Valkonen, R. G. Graversen, and G. Noer, 2020: A well-observed polar low analysed with a regional and a global weather-prediction model. *Quart. J. Roy. Meteor. Soc.*, **146**, 1740–1767, https://doi.org/10.1002/qj.3764.

Süld, J. K., A. Rasheed, J. Kristiansen, Ø. Øyvind Sætra, A. Carrasco, and T. Kvamsda, 2015: Mesoscale numerical modelling of Met-ocean interactions. *Energy Procedia*, **80**, 433–441, https://doi.org/10.1016/j.egypro.2015.11.447.

Valcke, S., T. Craig, and L. Coquart, 2015: OASIS3-MCT User Guide. OASIS, accessed 23 April 2018, http://oasis.enes.org.

Voldoire, A., and Coauthors, 2017: SURFEX v8.0 interface with OASIS3-MCT to couple atmosphere with hydrology, ocean, waves and sea-ice models, from coastal to global scales. *Geosci. Model Dev.*, **10**, 4207–4227, https://doi.org/10.5194/gmd-10-4207-2017.

Wahle, K., J. Staneva, W. Koch, L. Fenoglio-Marc, H. T. Ho-Hagemann, and E. V. Stanev, 2017: An atmosphere-wave regional coupled model: Improving predictions of wave heights and surface winds in the southern North Sea. *Ocean Sci.*, **13**, 289–301, https://doi.org/10.5194/os-13-289-2017.

WAVEWATCH III Development Group, 2016: User manual and system documentation of WAVEWATCH III version 5.16. Tech. Note 329, 326 pp., https://github.com/NOAA-EMC/WW3/wiki/WAVEWATCH-III-User-Guide.

Wu, L., 2021: Effect of atmosphere-wave-ocean/ice interactions on a polar low simulation over the Barents Sea. *Atmos. Res.*, **248**, 105183, https://doi.org/10.1016/j.atmosres.2020.105183.

——, Ø. Breivik, and A. Rutgersson, 2019: Ocean-wave-atmosphere interaction processes in a fully coupled modeling system. *J. Adv. Model. Earth Syst.*, **11**, 3852–3874, https://doi.org/10.1029/2019MS001761.

Zheng, K., J. Sun, C. Guan, and W. Shao, 2016: Analysis of the global swell and wind sea energy distribution using WAVEWATCH III. *Adv. Meteor.*, **2016**, 8419580, https://doi.org/10.1155/2016/8419580.